European Journal of Chemistry

Check for updates

View Journal Online
View Article Online

Halide bridged organophosphorus complexes of HgX_2 (X: I, Br and Cl): Synthesis, structure and theoretical studies

Jahangir Mondal, Amit Kumar Manna and Goutam Kumar Patra *

Department of Chemistry, School of Physical Sciences, Guru Ghasidas Vishwavidyalaya, Bilaspur, Chhattisgarh, 495009, India
mailtobapi88@gmail.com (J.M.), amitmanna51@gmail.com (A.K.M.), goutam.patra@ggu.ac.in (G.K.P.)

* *Corresponding author at: Department of Chemistry, School of Physical Sciences, Guru Ghasidas Vishwavidyalaya, Bilaspur, Chhattisgarh, 495009, India. e-mail: goutam.patra@ggu.ac.in (G.K. Patra).*

RESEARCH ARTICLE

10.5155/eurjchem.12.1.23-31.2039

Received: 31 August 2020
Received in revised form: 07 December 2020
Accepted: 20 December 2020
Published online: 31 March 2021
Printed: 31 March 2021

KEYWORDS

DFT
Mercury halides
X-ray crystal structure
Hirshfeld surface studies
Halide bridged complexes
Triphenyl phosphine ligand

ABSTRACT

Three organophosphorus mercury (II) coordination compounds $[Hg_2(\mu\text{-}X)_2X_2(PPh_3)_2]$ {X: I (1), Br (2), and Cl (3)} have been synthesized by the reaction of mercury (II) halides with triphenylphosphine. The prepared complexes were characterized by spectroscopic techniques as well as by elemental analysis. The crystal structure of $[Hg_2(\mu\text{-}I)_2I_2(PPh_3)_2]$ (1) was obtained by single-crystal X-ray diffraction study. Crystal data for $[Hg_2(\mu\text{-}I)_2I_2(PPh_3)_2]$, $C_{36}H_{30}Hg_2I_4P_2$: Monoclinic, space group $P2_1/c$ (no. 14), a = 19.2115(13) Å, b = 11.1291(8) Å, c = 19.0599(14) Å, β = 90.461(2)°, V = 4075.0(5) Å^3, Z = 4, T = 293.15 K, μ (MoKα) = 10.657 mm^{-1}, *Dcalc* = 2.336 g/cm^3, 46095 reflections measured (4.23° ≤ 2Θ ≤ 49.994°), 7182 unique (R_{int} = 0.0563, R_{sigma} = 0.0365) which were used in all calculations. The final R_1 was 0.0322 (I > 2σ(I)) and wR_2 was 0.0780 (all data). The single crystal analysis of $[Hg_2(\mu\text{-}I)_2I_2(PPh_3)_2]$ complex revealed that it has dimeric structure with bridged halides. $[Hg_2(\mu\text{-}I)_2I_2(PPh_3)_2]$ complex has also a supramolecular arrangement through I···H-C interactions. The crystal packing and supramolecular features of these coordination compounds have also been studied using geometrical analysis, Hirshfeld surface analysis and DFT studies. Hirshfeld surface analysis indicated that H···H (49.3%), C···H (10.6%), and I···H (12.8%) interactions are the primary contributors to the intermolecular stabilization in the crystal. The equilibrium geometries of the studied complexes are investigated theoretically at the B3LYP/LANL2DZ level of theory. The calculated energy gap between HOMO-LUMO orbitals for complexes 1, 2, and 3 are in the trend of complex 3 > 2 > 1.

Cite this: *Eur. J. Chem.* **2021**, *12(1)*, 23-31 **Journal website**: www.eurjchem.com

1. Introduction

Mercury is a toxic and hazardous heavy metal, and it can easily coordinate with S, N, and P-containing ligands. Mercury phosphine complexes embody a wide range of structural types [1]. Besides, mercury (II) halides are compounds of current interest due to their possible applications as materials with nonlinear optical properties [2]. Due to these features, understanding the coordination chemistry of the mercury (II) ion is crucial for the rational development of materials with specific biological and physical properties [2,3]. The tolerance for many different coordination numbers and geometries is typical of the coordination chemistry of mercury (II) ions. The mercury (II) ion is a distinctly 'soft' cation, showing a strong preference for Cl, Br, I, P, S and N-type ligands [4,5]. Recently, efforts have been made to better understand the coordination properties of this metal ion. In the course of these investigations, a quite unexpected sevenfold coordination of a hydrated mercury (II) complex in aqueous solution has been revealed [6]. Moreover, there are some examples reported in the literature describing the influence of weak intermolecular interactions on the coordination geometry of the metal center and the formation of unusual coordination geometries around the mercury (II) ion [7-15]. Several of phosphate acid complexes have been studied as promising materials for second harmonic generation [16,17]. A literature survey reveals that to the best of our knowledge, no DFT wavenumber and structural parameter calculations of the title compound have been reported so far. This inadequacy observed in literature and the absence of the center of symmetry of the studied compound encouraged us to undertake this experimental and theoretical work. In recent years, density functional theory (DFT) has been a shooting star in theoretical modeling [18-25]. The development of a better exchange-correlation functional made it possible to calculate many molecular properties with comparable accuracy to traditional correlated ab initio methods, with more favorable computational costs [24]. Literature survey revealed that the DFT has a great accuracy in reproducing the experimental values in terms of geometry, dipole moment, vibrational frequency, etc. [26,27]. Hirshfeld surface-based tools appear as a novel approach to this end [28-34].

We report here the synthesis and characterization of three halide bridged mercury (II) complexes $[Hg_2(\mu\text{-}X)_2X_2(PPh_3)_2]$ {X: I (**1**), Br (**2**), and Cl (**3**)} containing the triphenylphosphine ligand. The single crystal structure of complex **1** was obtained and its simulated powder pattern was compared with the powder X-ray diffraction (XRD) data of the other two derivatives (**2** and **3**). We also compared obtained data with the

ISSN 2153-2249 (Print) / ISSN 2153-2257 (Online) – Copyright © 2021 The Authors – Atlanta Publishing House LLC – Printed in the USA.
This work is published and licensed by Atlanta Publishing House LLC – CC BY NC – Some Rights Reserved.
https://dx.doi.org/10.5155/eurjchem.12.1.23-31.2039

literature [35]. These coordination compounds were studied using geometrical analysis, Hirshfeld surface analysis, and DFT studies, helping us to compare with each other. The equilibrium geometry and other properties of the studied complexes are investigated theoretically at the B3LYP/LANL2DZ level of theory.

2. Experimental

2.1. Materials and physical measurements

All chemicals used in this study were purchased from Aldrich Chemical Company, USA, and Across Chemical Company, USA, and used without further purification unless otherwise mentioned. The melting point was determined by an electro-thermal IA9000 series digital melting point apparatus and is uncorrected. Microanalyses were carried out using a Perkin-Elmer 2400II elemental analyzer. Infrared (IR) data was collected on Nicolet Magna-IR (Series II) by KBr disc by scanning from 4000 to 400 cm^{-1}. Solution electronic spectra (200-800 nm) were recorded by Shimadzu UV-160A spectrophotometer using dimethylformamide (DMF) as solvent. ^1H and ^{13}C NMR data were recorded on a Bruker Advance 300 MHz and 75 MHz spectrometer, respectively, in DMSO-d_6 as solvent and TMS as standard. X-ray powder patterns are collected on a Philips PW-1710 automated diffractometer.

2.2. Synthesis of the complexes

2.2.1. Synthesis of $[Hg_2(\mu\text{-}I)_2I_2(PPh_3)_2]$ (1)

Triphenylphosphine (0.262 g, 1 mmol) was dissolved in CH_3CN (40 mL). To this colorless solution, mercury iodide (0.454 g, 1 mmol) in 30 mL CH_2Cl_2 was added. The reaction mixture was stirred at room temperature for 3 h to obtain a clear solution. The solution was evaporated to obtain white, blocked shaped single crystals, suitable for X-ray analysis. The obtained products were washed with 5 mL of CH_2Cl_2 and dried in air. Color: White. Yield: 80.75%. M.p.: >200 °C. FT-IR (KBr, ν, cm^{-1}): 3429(b), 2919 (w), 2362 (s), 2162(vs), 2013 (s), 1917 (m), 1507 (m), 1366 (m), 844 (m), 405 (vs). ^1H NMR (300 MHz, DMSO-d_6, δ, ppm): 7.51-8.67 (m, 15H, Ar-H). ^{13}C NMR (75 MHz, DMSO-d_6, δ, ppm): 126.04,129.61, 133.38, 133.49. Anal. calcd. for $C_{36}H_{30}Hg_2I_4P_2$: C, 30.17; H, 2.11. Found: C, 30.58; H, 2.05%. UV/Vis (DMF, λ_{max}, nm, (ε)): 292 (0.062).

2.2.2. Synthesis of $[Hg_2(\mu\text{-}Br)_2Br_2(PPh_3)_2]$ (2)

Triphenylphosphine (0.262 g, 1 mmol) was dissolved in CH_3CN (40 mL). To this colorless solution, mercury bromide (0.360 g, 1 mmol) in 30 mL CH_2Cl_2 was added. The reaction mixture was stirred at room temperature for 3 h to obtain a clear solution. The solution was evaporated to obtain white, blocked shaped single crystals, suitable for X-ray analysis. The obtained products were washed with 5 mL of CH_2Cl_2 and dried in air. Color: White. Yield: 79%. M.p.: >200 °C. FT-IR (KBr, ν, cm^{-1}): 3415(b), 3046 (w), 2366 (s), 2164 (vs), 2019 (s) 1931 (m), 150 5(s), 1374 (m), 1105 (w), 869 (s), 435 (w). ^1H NMR (300 MHz, DMSO-d_6, δ, ppm): 7.96-8.75 (m, 15H, Ar-H). ^{13}C NMR (75 MHz, DMSO-d_6, δ, ppm): 127.17,130.33, 133.89, 134.52. Anal. calcd. for $C_{36}H_{30}Hg_2Br_4P_2$: C, 34.72; H, 2.43. Found: C, 34.99; H, 2.51%. UV/Vis (DMF, λ_{max}, nm, (ε)): 295 (0.060).

2.2.3. Synthesis of $[Hg_2(\mu\text{-}Cl)_2Cl_2(PPh_3)_2]$ (3)

Triphenylphosphine (0.262 g, 1 mmol) was dissolved in CH_3CN (40 mL). To this colorless solution, mercury chloride (0.270 g, 1 mmol) in 30 mL CH_2Cl_2 was added. The reaction mixture was stirred at room temperature for 3 h to obtain a clear solution. The solution was evaporated to obtain white, blocked shaped single crystals, suitable for X-ray analysis. The obtained products were washed with 5 mL of CH_2Cl_2 and dried in air. Color: White. Yield: 74.72%. M.p.: >200 °C. FT-IR (KBr, ν, cm^{-1}): 3392 (b), 3042 (w), 2361 (s), 2169 (vs), 2014 (s), 1921 (m), 1545 (m), 1506 (s), 1366 (m), 1248 (w), 864 (s), 438(w). ^1H NMR (300 MHz, DMSO-d_6, δ, ppm): 7.57-8.73 (m, 15H, Ar-H). ^{13}C NMR (75 MHz, DMSO-d_6, δ, ppm): 126.25, 129.83, 133.59, 133.72. Anal. calcd. for $C_{36}H_{30}Hg_2Cl_4P_2$: C, 40.50; H, 2.83. Found: C, 40.67; H, 2.69%. UV/Vis (DMF, λ_{max}, nm, (ε)): 297 (0.061).

2.3. X-Ray crystallography

X-ray single crystal data are collected at room temperature (298 K) using MoKα (λ = 0.71073 Å) radiation on a Bruker APEX II diffractometer equipped with CCD area detector. Data collection, data reduction, structure solution/refinement are carried out using the software package of SMART APEX [36]. The structures are solved by direct methods (SHELXS-97) and standard Fourier techniques, and refined on F^2 using full matrix least squares procedures using the SHELX-97 package [37] incorporated in WinGX [38]. Non-hydrogen atoms are treated anisotropically. The hydrogen atoms are geometrically fixed. The crystallographic details of complex **1** have been summarized in Table 1, and the selected bond lengths and angles of complex **1** are listed in Table 2.

2.4. Theoretical calculations

The quantum chemical calculations were carried out using Gaussian 09 program [39]. Possible ground state structures have been optimized with density functional theory (DFT) at B3LYP/LANL2DZ. GaussView 5 program [40] was used for the visualization of the studied systems.

2.5. Hirshfeld Surface calculations

Hirshfeld surface analysis helps as a powerful set-up for obtaining additional insight into the intermolecular interaction of molecular crystals. The size and shape of Hirshfeld surface allows the qualitative and quantitative study and imagining of intermolecular close contacts in molecular crystals [41]. The Hirshfeld surface enclosing a molecule is defined by a set of points in 3D space where the contribution to the electron density from the molecule of interest is equal to the contribution from all other molecules. Molecular Hirshfeld surfaces are constructed based on the electron distribution calculated as the sum of spherical atom electron densities [42]. Thus, an isosurface is obtained, and for each point of the isosurface two distances can be defined: d_e, the distance from the point to the nearest atom outside to the surface, and d_i, the distance to the nearest atom inside to the surface. Moreover, the identification of the regions of particular importance to intermolecular interactions is obtained by mapping normalized contact distance (d_{norm}), expressed as: $d_{norm} = (d_i - r_i^{vdw})/r_i^{vdw} + (d_e - r_e^{vdw})/r_e^{vdw}$; where r_i^{vdw} and r_e^{vdw} are the van der Waals radii of the atoms [43]. The value of d_{norm} is negative or positive when intermolecular contacts are shorter or longer than r^{vdw}, respectively. Graphical plots of the molecular Hirshfeld surfaces mapped with d_{norm} employ the red-white-blue color scheme, where red color indicates the shorter intermolecular contacts, white color show the contacts around the r^{vdw} separation, and blue color is used to indicate the longer contact distances. Because of the symmetry between d_e and d_i in the expression for d_{norm}, where two Hirshfeld surfaces touch, both will display a red spot identical in color intensity as well as size and shape [44].

Table 1. Crystal data and structure refinement for $[Hg_2(\mu\text{-}I)_2I_2(PPh_3)_2]$ (**1**).

Compound	**$[Hg_2(\mu\text{-}I)_2I_2(PPh_3)_2]$ (1)**
CCDC No	1053733
Empirical formula	$C_{36}H_{30}Hg_2I_4P_2$
Formula weight	1433.32
Temperature (K)	293.15
Crystal system	Monoclinic
Space group	$P2_1/c$
a (Å)	19.2115(13)
b (Å)	11.1291(8)
c (Å)	19.0599(14)
β (°)	90.461(2)
Volume (Å^3)	4075.0(5)
Z	4
ρ_{calc} (g/cm^3)	2.336
μ (mm^{-1})	10.657
F(000)	2592.0
Crystal size (mm^3)	0.21 × 0.17 × 0.11
Radiation	MoKα (λ = 0.71073)
2Θ range for data collection (°)	4.23 to 49.994
Index ranges	$-22 \le h \le 22$, $-13 \le k \le 12$, $-22 \le l \le 22$
Reflections collected	46095
Independent reflections	7182 [R_{int} = 0.0563, R_{sigma} = 0.0365]
Data/restraints/parameters	7182/0/397
Goodness-of-fit on F^2	1.012
Final R indexes [I>=2σ (I)]	R_1 = 0.0322, wR_2 = 0.0700
Final R indexes [all data]	R_1 = 0.0494, wR_2 = 0.0780
Largest diff. peak/hole (e.Å^{-3})	0.84/-1.22

Table 2. Selected bond distances (Å) and angles (°) for complexes **1**, **2** and **3**.

Comp.	**Bond distance**	**Experimental X-ray diffraction**	**Theoretical B3LYP/ LANL2DZ**	**Bond angle**	**Experimental X-ray diffraction**	**Theoretical B3LYP/ LANL2DZ**	**Bond angle**	**Experimental X-ray diffraction**	**Theoretical B3LYP/ LANL2DZ**
1	Hg1-I1	2.8397(6)	2.839	I1-Hg1-I2	95.827(15)	95.830	C1-P1-Hg1	110.4(2)	110.4
	Hg1-I2	2.9539(6)	2.953	I3-Hg1-I1	110.072(19)	110.073	C7-P1-Hg1	110.9(2)	111.1
	Hg1-I3	2.6745(6)	2.674	I3-Hg1-I2	106.570(18)	106.580	C13-P1-Hg1	113.7(2)	114.0
	Hg1-P1	2.4739(17)	2.474	P1-Hg1-I1	110.24(4)	110.240	C19-P2-Hg2	112.4(2)	112.4
	Hg2-I1	2.9784(6)	2.978	P1-Hg1-I2	102.71(4)	102.711	C25-P2-Hg2	111.0(2)	111.2
	Hg2-I2	2.8506(6)	2.851	P1-Hg1-I3	126.53(4)	126.532	C31-P2-Hg2	109.9(2)	110.2
	Hg2-I4	2.6673(5)	2.667	I2-Hg2-I1	95.050(15)	95.051	C14-C13-P1	122.5(6)	122.5
	Hg2-P2	2.4616(17)	2.462	I4-Hg2-I1	107.988(18)	108.025	C18-C13-P1	118.0(6)	118.0
	P1-C1	1.799(7)	1.800	I4-Hg2-I2	106.700(18)	107.120	C2-C1-P1	117.8(5)	118.1
	P1-C7	1.794(7)	1.794	P2-Hg2-I1	100.57(4)	100.57	C6-C1-P1	122.4(6)	122.4
	P1-C13	1.792(7)	1.792	P2-Hg2-I2	112.46(5)	112.460	C20-C19-P2	122.3(6)	122.3
	P2-C19	1.803(7)	1.803	P2-Hg2-I4	128.53(4)	128.532	C24-C19-P2	118.3(6)	118.3
	P2-C25	1.799(7)	1.799	Hg1-I1-Hg2	84.432(14)	84.432	C26-C25-P2	122.3(6)	122.3
	P2-C31	1.811(8)	1.811	Hg2-I2-Hg1	84.691(14)	84.691	C30-C25-P2	118.3(5)	118.3
2	Hg1-Br1		2.850	Br1-Hg1-Br2		95.050	C1-P1-Hg1		109.9
	Hg1-Br2		2.978	Br3-Hg1-Br1		106.584	C7-P1-Hg1		110.8
	Hg1-Br3		2.580	Br3-Hg1-Br2		108.081	C13-P1-Hg1		114.0
	Hg1-P1		2.461	P1-Hg1-Br1		126.579	C19-P2-Hg2		112.1
	Hg2-Br1		2.839	P1-Hg1-Br2		102.703	C25-P2-Hg2		110.9
	Hg2-Br2		2.954	P1-Hg1-Br3		100.569	C31-P2-Hg2		110.2
	Hg2-Br4		2.580	Br2-Hg2-Br1		108.021	C14-C13-P1		122.3
	Hg2-P2		2.474	Br4-Hg2-Br1		112.442	C18-C13-P1		122.2
3	Hg1-Cl1		2.839	Cl1-Hg1-Cl2		102.703	C1-P1-Hg1		109.7
	Hg1-Cl2		2.954	Cl3-Hg1-Cl1		95.837	C7-P1-Hg1		110.6
	Hg1-Cl3		2.430	Cl3-Hg1-Cl2		95.050	C13-P1-Hg1		113.9
	Hg1-P1		2.474	P1-Hg1-Cl1		126.579	C19-P2-Hg2		111.9
	Hg2-Cl1		2.850	P1-Hg1-Cl2		110.207	C25-P2-Hg2		110.6
	Hg2-Cl2		2.978	P1-Hg1-Cl3		100.569	C31-P2-Hg2		110.0
	Hg2-Cl4		2.954	Cl2-Hg2-Cl1		84.679	C14-C13-P1		122.1
	Hg2-P2		2.430	Cl4-Hg2-Cl1		84.434	C18-C13-P1		122.0

The combination of d_e and d_i in the form of a 2D fingerprint plot provides a summary of intermolecular contacts in the crystal and are in complement to the Hirshfeld surfaces. Such plots provide information about the intermolecular interactions in the immediate environment of each molecule in the asymmetric unit. Moreover, the close contacts between particular atom types can be highlighted in so-called resolved fingerprint plots, which allow the facile assignment of an intermolecular contact to a certain type of interaction and quantitatively summarize the nature and type of intermolecular contacts. Two additional colored properties (shape index and curvedness) based on the local curvature of the surface can also be specified. The Hirshfeld surfaces are mapped with d_{norm}, shape-index, curvedness and 2D fingerprint plots (full and resolved) presented in this paper were generated using Crystal Explorer 3.1 [45].

2.6. Molecular electrostatic potential

The molecular electrostatic potential (MEP) at a given point around a molecule can be defined in terms of the total charge distribution of the molecule and related to the dipole moments. It provides a method to understand the electron density which is useful for determining the electrophilic reactivity and nucleophilic reactivity as well as hydrogen-bonding interactions [46,47].

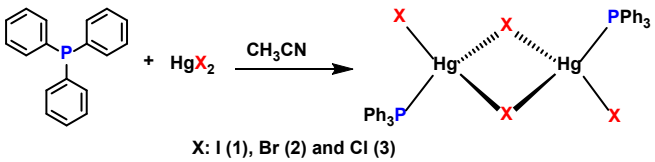

Scheme 1. Synthetic routes for the synthesis of complexes **1**, **2** and **3**.

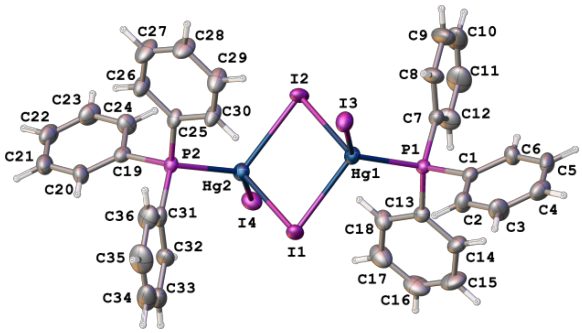

Figure 1. The molecular structure of $[Hg_2(\mu\text{-}I)_2I_2(PPh_3)_2]$ (**1**) with atom labeling scheme.

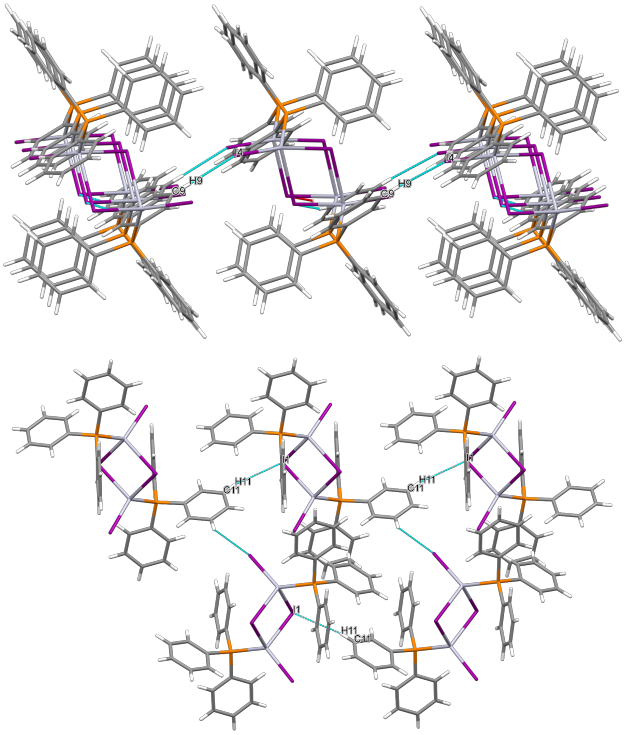

Figure 2. Supramolecular arrangements in $[Hg_2(\mu\text{-}I)_2I_2(PPh_3)_2]$ (**1**) through I···H-C-interaction.

3. Results and discussion

3.1. Synthesis aspects of the complexes

The organophosphorus complexes **1**, **2**, and **3** have been synthesized as white crystalline solids by the reaction of HgX_2 (X: I, Br, and Cl) and PPh_3 in 1:1 proportion in good yield in acetonitrile medium (Scheme 1). Earlier, Dadrass *et al.* [35] reported the syntheses of these complexes, but their synthetic methods were more tedious and less economical. These had been prepared by the nucleophilic substitution reaction of triphenylphosphine ligand with tri(*p*-tolyl)phosphinehalide complexes using dry solvent methanol and diethyl ether, and recrystallized from chloroform diethyl ether. Its reaction time was also much longer than our reaction time.

3.2. Structural description of complex 1

Single crystal XRD analysis revealed that the $[Hg_2(\mu\text{-}I)_2I_2(PPh_3)_2]$ (**1**) crystallized in monoclinic $P2_1/c$ space group. The molecular structure of the complex is shown in Figure 1. The complex **1** is stabilized by C-H···I interactions (C9-H9···I4 and C11-H11···I1) (Figure 2). The sp^3 hybridized Hg (II) ion in the complex **1** adopted a tetrahedral coordination environment with one short Hg–I bond at distance 2.6745(6) Å, one Hg–P bond at distance 2.4739(17) Å and two asymmetric bridging Hg–I bonds at distances 2.8397(6) and 2.9539(6) Å.

Table 3. HOMO and LUMO energy values for complexes **1**, **2** and **3**.

Complex	HOMO (eV)	LUMO (eV)	Band Gap (HOMO-LUMO) (eV)
$[Hg_2(\mu\text{-}I)_2I_2(PPh_3)_2]$ (**1**)	-8.2737	-0.7877	7.4860
$[Hg_2(\mu\text{-}Br)_2Br_2(PPh_3)_2]$ (**2**)	-9.0364	-0.8380	8.1984
$[Hg_2(\mu\text{-}Cl)_2Cl_2(PPh_3)_2]$ (**3**)	-9.5049	-0.8525	8.6524

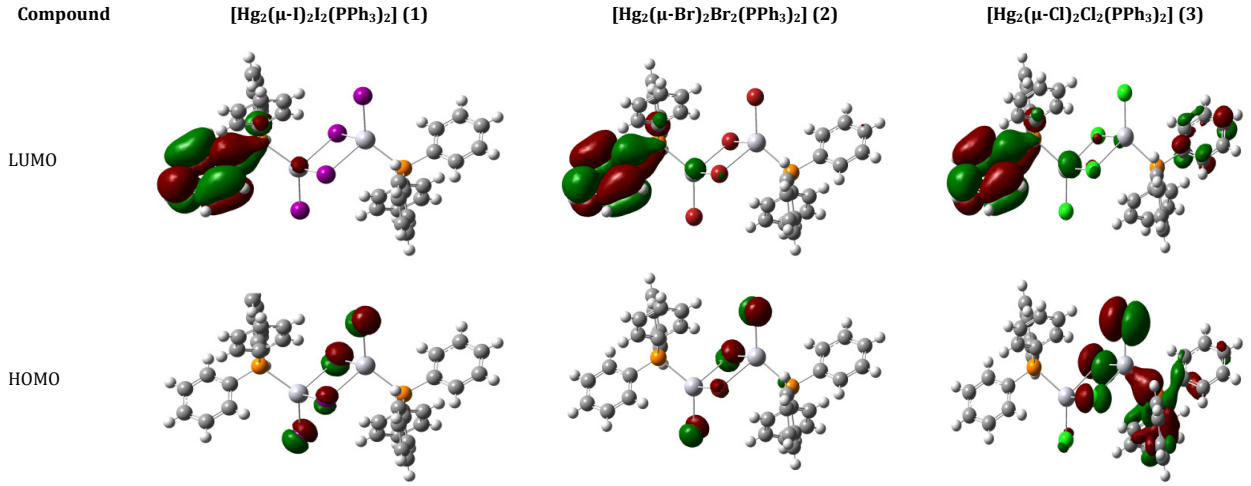

Figure 3. Surface plots of HOMO and LUMO in complexes **1**, **2** and **3**.

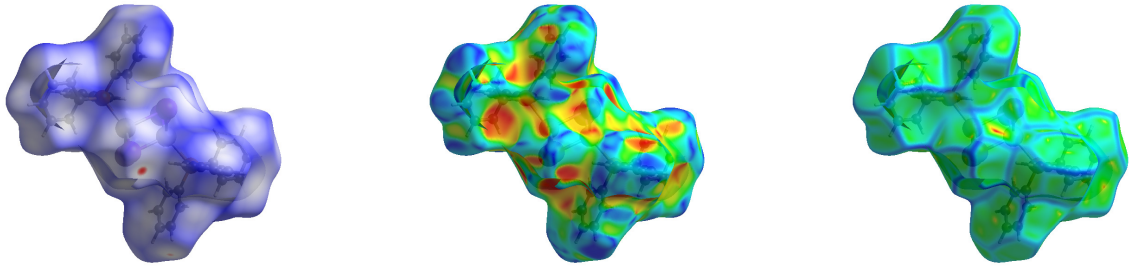

(a) (b) (c)

Figure 4. Hirshfeld surfaces of complex **1**, (a) 3D d_{norm} surface, (b) Shape index, (c) curvedness.

The internuclear distances between mercury atoms were found to be 3.911(2) Å, which was much longer than the sum of van Der Waals radius (1.50 Å) of the two mercury atoms [35,48]. This indicated that the absence of significant bonding interactions between the mercury atoms in the molecular structure of complex **1**. Some other important bond lengths and bond angles represented in Table 2.

3.3. Theoretical investigations

The geometry of the organophosphorus complexes, $[Hg_2(\mu\text{-}X)_2X_2(PPh_3)_2]$ {X: I (**1**), Br (**2**), and Cl (**3**)} have been optimized and the calculated structures have C1 symmetry. The final optimized structure parameters are listed in Table 2. The highest occupied molecular orbital (HOMO)-the lowest unoccupied molecular orbital (LUMO) gap is an important parameter to characterize the chemical reactivity and kinetic stability of any compound [49]. It is a well-known fact that the energy gap retains a close connection with some molecular properties [50]. A soft molecule has a small HOMO-LUMO gap energy, more polarizable, high chemical reactivity, and low kinetic stability. The surface plots of HOMO and LUMO of the complexes **1**, **2**, and **3** have been displayed in Figure 3 with their energy values. The energies of LUMO and HOMO of the complexes **1**, **2**, and **3** have been shown in Table 3. The calculated energy gap between the latter orbitals for complex **1** containing iodine is smaller than that for other complexes and the trend is as Cl (**3**) > Br (**2**) > I (**1**). The most important requisites in this kind of interaction are contributed from the partial charge transfer between the highest occupied molecular orbital (HOMO) of one component and the lowest unoccupied molecular orbital (LUMO) of another.

3.4. Molecular Hirshfeld surfaces

The Hirshfeld surface emerged from an attempt to define the space occupied by a molecule in a crystal for the purpose of partitioning the crystal electron density into molecular fragments. The Hirshfeld surface is a suitable tool for describing the surface characteristics of molecules. The molecular Hirshfeld surfaces of complex **1** were generated using a standard (high) surface resolution with the 3D d_{norm} surfaces mapped over a fixed color scale of -0.22 (red) to 1.4 Å (blue). The shape index mapped in the color range of -0.99 to 1.0, and Curvedness was in the range of -4.0 to 0.4. The surfaces were shown to be transparent to allow visualization of the molecular moiety in a similar orientation for all structures around which they were calculated. The molecular Hirshfeld surface (d_{norm}, *Shape index,* and *Curvedness*) of complex **1** has been shown in Figure 4.

The Hirshfeld surface analysis showed that complex **1** has H···H, C···H, and I···H interactions with 49.3, 10.6, and 12.8%, respectively, which revealed that the main intermolecular interactions were H···H. The C···H and I···H interactions were represented by a small area in the 2D fingerprint region plot (Figure 5).

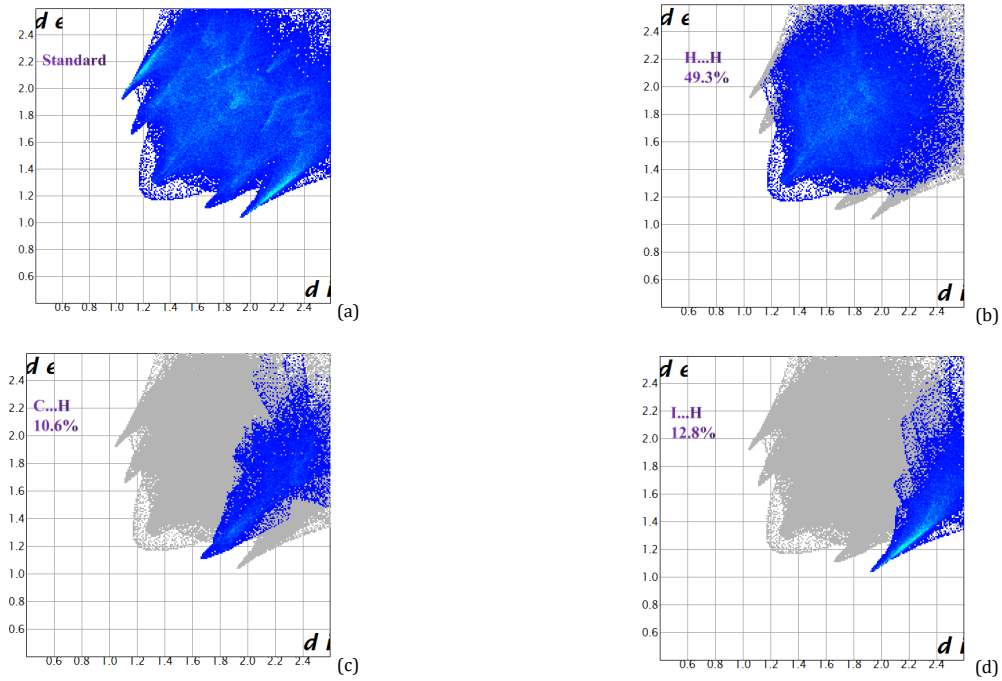

Figure 5. 2D fingerprint plots of complex **1**, (a) standard full, (b) resolved into H···H, (c) resolved into C···H and (d) I···H contacts, showing the percentages of contacts contributing to the total Hirshfeld surface area of the molecule.

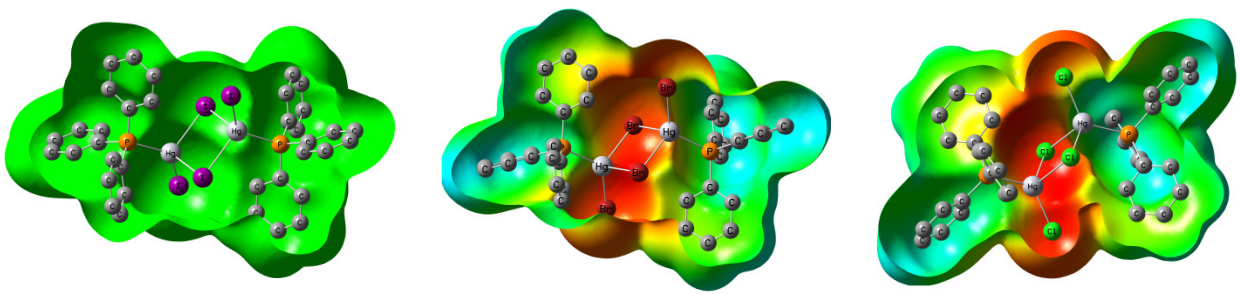

[$Hg_2(\mu\text{-}I)_2I_2(PPh_3)_2$] (1) **[$Hg_2(\mu\text{-}Br)_2Br_2(PPh_3)_2$] (2)** **[$Hg_2(\mu\text{-}Cl)_2Cl_2(PPh_3)_2$] (3)**

Figure 6. Molecular electrostatic potential (MEP) of complexes **1**, **2**, and **3**.

Therefore, this finding indicates that the significance of these contacts in the packing arrangement of the crystal structure of complex **1**. Based on these findings, the detailed model may be constructed showing the prominent short-range intermolecular contacts that are responsible for the packing arrangement and formation of the three-dimensional network structure.

3.5. Molecular electrostatic potential

The molecular electrostatic potential (MEP) at a given point p(x,y,z) in the vicinity of a molecule is the force acting on a positive test charge (a proton) located at p through the electrical charge cloud generated through the molecules electrons and nuclei. Different values of the electrostatic potential at the surface are represented by different colors. The potential increases in the following order: red < orange < yellow < green < blue. The negative electrostatic potential corresponds to an attraction of a proton by the aggregate electron density in the molecule (shades of red and yellow) and the positive electrostatic potential corresponds to the repulsion of a proton by the nuclei (shades of blue). The molecular electrostatic potentials (MEP) of the organophosphorous complexes **1**, **2**, and **3** are shown in Figure 6. One-third of the molecules of complexes **2** and **3** have reddish yellow in color because of the unequal distribution of electron density over these molecules. As can be seen from Figure 6, the negative electrostatic potential regions are mainly localized over the halide group and are possible sites for electrophilic attack except [$Hg_2(\mu\text{-}I)_2I_2(PPh_3)_2$].

3.6. Mulliken atomic charge

The Mulliken charges quantify how the electronic structure changes under atomic displacement; therefore, it is related directly to the chemical bonds present in the molecule. The Mulliken charges are explicitly sensitive to the basis set choice. In principle, a complete basis set for a molecule can be spanned by placing a large set of functions on a single atom. In the Mulliken scheme, all the electrons would then be assigned to this atom. The method thus has no complete basis set limit, as the exact value depends on the way the limit is approached. This also means that the charges are ill defined, as there is no exact answer. As a result, the basis set convergence of the charges does not exist, and different basis set families may yield drastically different results. Mulliken charges affect the dipole moment, polarizability, electronic structure, and more properties of molecular systems.

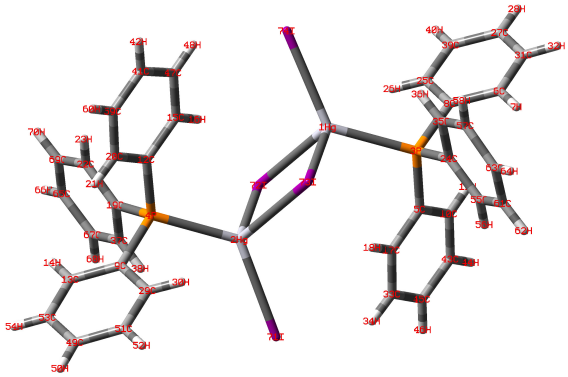

Figure 7. Molecular structure of complex **1** with atom labelled form for Mulliken atomic charge.

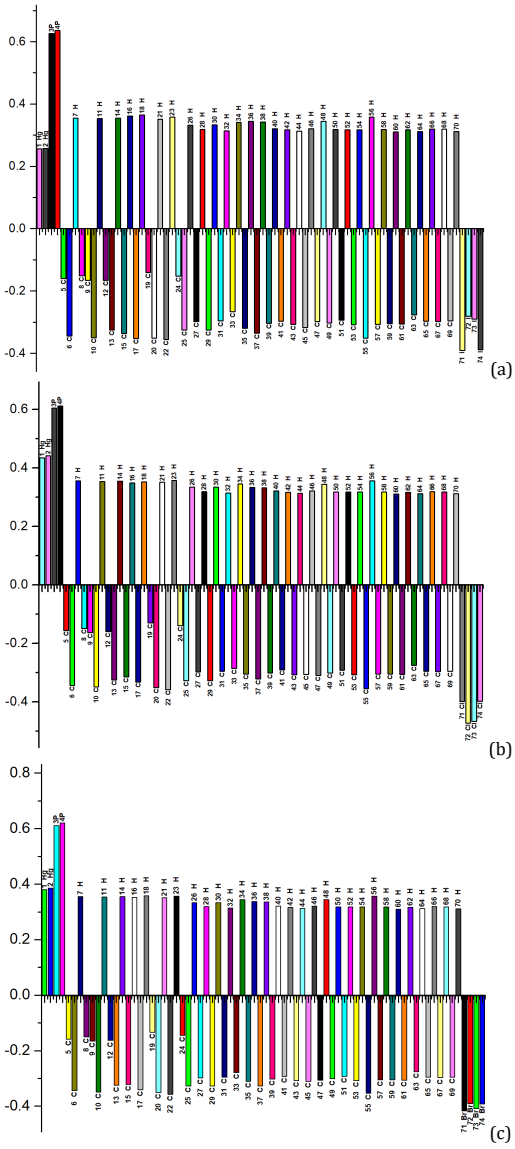

Figure 8. Mulliken atomic charge distribution of the organophosphorus complexes **1** (a), **2** (b) and **3** (c).

Molecular structure of complex **1** with atom labelled form for Mulliken atomic charge is shown in Figure 7. The Mulliken population analysis for the complexes is calculated using B3LYP/LANL2DZ. The Mulliken charge distribution structure of the complexes is shown in Figure 8.

3.7. The powder XRD of the complexes 1, 2, and 3

We have obtained single crystal X-ray diffraction quality crystals only for the complex **1**. From the X-ray analysis, its structure is a centrosymmetric dimeric structure and metal center bridged with two iodide groups.

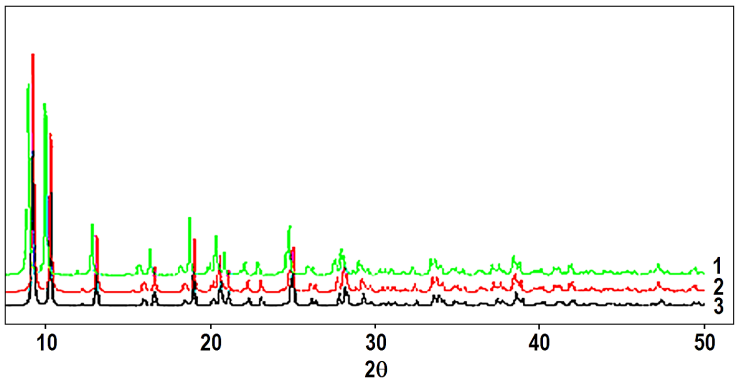

Figure 9. Comparison of powdered XRD of the complexes **1**, **2** and **3**.

For the rest two complexes **2** and **3**, we have prepared the semicrystalline solid. To determine the structures of complexes **2** and **3**, we have matched the powder diffraction data of complexes **2** and **3** with the simulated powder data obtained from the single crystals of complex **1** and found that they are in good agreement (Figure 9). Moreover, the theoretically calculated bond distances and bond angles of complexes **2** and **3** are also in good agreement with those data of the single crystal structure of complex **1**. Therefore, we can conclude that complexes **2** and **3** are also halide bridged dimers.

4. Conclusion

Herein, exploiting the reaction between triphenyl phosphine and mercury halides, organophosphorus compounds of mercury (II) halides (**1**, **2**, and **3**) have been synthesized and characterized by elemental analysis, FTIR, NMR and DFT studies. $[Hg_2(\mu\text{-}I)_2I_2(PPh_3)_2]$ (**1**) has been also characterized by a single crystal X-ray diffraction study. The metal centers in complex **1** were bridged by two iodide groups. The matching of X-ray powder patterns of the prepared complexes revealed that complexes **2** and **3** are also a similar structure with complex **1**. The Hirshfeld surface analysis of the complex **1** showed H···H, C···H, and I···H interactions of 49.3, 10.6, and 12.8%, respectively. The calculated energy gap between HOMO-LUMO orbitals for complexes **1**, **2**, and **3** are in the trend of **3** > **2** > **1**.

Acknowledgements

Goutam Kumar Patra would like to thank the Department of Science and Technology, Government of India, New Delhi, for financial support (File Nos. SR/FST/CSI-264/2014 and EMR/2017/0001789).

Supporting information

CCDC-1053733 contains the supplementary crystallographic data for this paper. These data can be obtained free of charge via https://www.ccdc.cam.ac.uk/structures/, or by e-mailing data_request@ccdc.cam.ac.uk, or by contacting The Cambridge Crystallographic Data Centre, 12 Union Road, Cambridge CB2 1EZ, UK; fax: +44(0)1223-336033.

Disclosure statement

Conflict of interest: The authors declare that they have no conflict of interest.
Author contributions: All authors contributed equally to this work.
Ethical approval: All ethical guidelines have been adhered.
Sample availability: Samples of the compounds are available from the author.

ORCID

Jahangir Mondal
https://orcid.org/0000-0001-9867-5193
Amit Kumar Manna
https://orcid.org/0000-0002-9605-2168
Goutam Kumar Patra
https://orcid.org/0000-0003-3151-0284

References

[1]. Jennette, K. W. *Environ. Health Perspec.* **1981**, *40*, 233–252.
[2]. Dang, Y.; Meng, X.; Jiang, K.; Zhong, C.; Chen, X.; Qin, J. *Dalton Trans.* **2013**, *42 (27)*, 9893-9897.
[3]. Tanaka, Y.; Kondo, J.; Sychrovsky, V.; Sebera, J.; Dairaku, T.; Saneyoshi, H.; Urata, H.; Torigoe, H.; Ono, A. *Chem. Commun.* **2015**, *51 (98)*, 17343–17360.
[4]. Cotton, F. A.; Wilkinson, G.; Murillo, C. A.; Bochmann, M. Advanced Inorganic Chemistry, 6th edition, John Wiley & Sons, 1999.
[5]. Grdenic, D. *Q. Rev. Chem. Soc.* **1965**, *19 (3)*, 303-328.
[6]. Chillemi, G.; Mancini, G.; Sanna, N.; Barone, V.; Della Longa, S.; Benfatto, M.; Pavel, N. V.; D'Angelo, P. *J. Am. Chem. Soc.* **2007**, *129 (17)*, 5430–5436.
[7]. Khavasi, H. R.; Tahrani, A. A. *CrystEngComm* **2013**, *15 (29)*, 5799-5812.
[8]. Khavasi, H. R.; Azizpoor Fard, M. *Cryst. Growth Des.* **2010**, *10 (4)*, 1892–1896.
[9]. Khavasi, H. R.; Mir Mohammad Sadegh, B. *Dalton Trans.* **2014**, *43 (14)*, 5564–5573.
[10]. Guidara, S.; Feki, H.; Abid, Y. *Spectrochim. Acta A* **2013**, *115*, 437–444.
[11]. Elleuch, N.; Ben Ahmed, A.; Feki, H.; Abid, Y.; Minot, C. *Spectrochim. Acta A* **2014**, *121*, 129–138.
[12]. Guidara, S.; Ahmed, A. B.; Abid, Y.; Feki, H. *Spectrochim. Acta A* **2014**, *127*, 275–285.
[13]. Ahmed, A. B.; Elleuch, N.; Feki, H.; Abid, Y.; Minot, C. *Spectrochim. Acta A* **2011**, *79 (3)*, 554–561.
[14]. Ahmed, A. B.; Feki, H.; Abid, Y.; Boughzala, H.; Minot, C. *Spectrochim. Acta A* **2010**, 75 (1), 293–298.
[15]. Ahmed, A. B.; Feki, H.; Abid, Y.; Minot, C. *Spectrochim. Acta A* **2010**, *75 (4)*, 1315–1320.
[16]. Ahmed, A. B.; Feki, H.; Abid, Y.; Boughzala, H.; Minot, C.; Mlayah, A. *J. Mol. Struct.* **2009**, *920 (1–3)*, 1–7.
[17]. Ahmed, A. B.; Feki, H.; Abid, Y.; Boughzala, H.; Mlayah, A. *J. Mol. Struct.* **2008**, *888 (1–3)*, 180–186.
[18]. Zyss, J. Molecular Nonlinear Optics Materials Physics and Devices, Academic Press, New York, 1994.
[19]. Jiang, M.; Fang, Q. *Adv. Mater.* **1999**, *11 (13)*, 1147–1151.
[20]. Angeli Mary, P. A.; Dhanuskodi, S. *Spectrochim. Acta A* **2001**, *57 (12)*, 2345–2353.
[21]. Rajendran, V.; Shyamala, D.; Loganayaki, M.; Ramasamy, P. *Mater. Lett.* **2007**, *61 (16)*, 3477–3479.
[22]. Jeyakumari, A. P.; Manivannan, S.; Dhanuskodi, S. *Spectrochim. Acta A* **2007**, 67 (1), 83–86.
[23]. Dong, X.; Minhua, J.; Zhongke, T. *Acta Chim. Sinica* **1983**, *41 (6)*, 570-573.
[24]. Mondal, J.; Mukherjee, A.; Patra, G. K. *Inorg. Chim. Acta* **2017**, *463*, 44–53.

[25]. Mondal, J.; Pal, P. K.; Mukherjee, A.; Patra, G. K. *Inorg. Chim. Acta* **2017**, *466*, 274–284.
[26]. De Proft, F.; Geerlings, P. *Chem. Rev.* **2001**, *101 (5)*, 1451–1464.
[27]. Fitzgerald, G.; Andzelm, J. *J. Phys. Chem.* **1991**, *95 (26)*, 10531–10534.
[28]. Tanak, H. *Int. J. Quantum Chem.* **2011**, *112 (11)*, 2392–2402.
[29]. Hyde, S.; Ninham, B. W.; Andersson, S.; Larsson, K.; Landh, T.; Blum, Z.; Lidin, S. The Mathematics of Curvature. In the Language of Shape; Elsevier, 1997; pp 1–42.
[30]. Spackman, M. A.; McKinnon, J. J. *CrystEngComm* **2002**, *4 (66)*, 378–392.
[31]. McKinnon, J. J.; Fabbiani, F. P. A.; Spackman, M. A. *Cryst. Growth Des.* **2007**, *7 (4)*, 755–769.
[32]. Moggach, S. A.; Parsons, S.; Wood, P. A. *Crystallogr. Rev.* **2008**, *14 (2)*, 143–184.
[33]. Parkin, A.; Barr, G.; Dong, W.; Gilmore, C. J.; Jayatilaka, D.; McKinnon, J. J.; Spackman, M. A.; Wilson, C. C. *CrystEngComm* **2007**, *9 (8)*, 648-652.
[34]. Barr, G.; Dong, W.; Gilmore, C. J.; Parkin, A.; Wilson, C. C. *J. Appl. Cryst.* **2005**, *38 (5)*, 833–841.
[35]. Dadrass, A.; Rahchamani, H. *J. Chil. Chem. Soc.* **2016**, *61 (2)*, 2968–2972.
[36]. Bruker. SAINT, SMART. Bruker AXS Inc., Madison, Wisconsin, USA, 2004.
[37]. Sheldrick, G. M. *Acta Cryst. Sect. A* **2007**, *64 (1)*, 112–122.
[38]. Farrugia, L. J. *J. Appl. Cryst.* **1999**, *32 (4)*, 837–838.
[39]. Frisch, M. J.; Trucks, G. W.; Schlegel, H. B.; Scuseria, G. E.; Robb, M. A.; Cheese-Man, J. R.; Montgomery Jr., J. A.; Vreven, T.; Kudin, K. N.; Burant, J. C.; Millam, J. M.; Iyengar, S. S.; Tomasi, J.; Barone, V.; Mennucci, B.; Cossi, M.; Scalmani, G.; Rega, N.; Petersson, G. A.; Nakatsuji, H.; Hada, M.; Ehara, M.; Toyota, K.; Fukuda, R.; Hasegawa, J.; Ishida, M.; Nakajima, T.; Honda, Y.; Kitao, O.; Nakai, H.; Klene, M.; Li, X.; Knox, J. E.; Hratchian, H. P.; Cross, J. B.; Bakken, V.; Adamo, C.; Jaramillo, J.; Gomperts, R.; Stratmann, R. E.; Yazyev, O.; Austin, A. J.; Cammi, R.; Pomelli, C.; Ochterski, J. W.; Ayala, P. Y.; Morokuma, K.; Voth, G.; Salvador, A. P.; Dannenberg, J. J.; Zakrzewski, V. G.; Dapprich, S.; Daniels, A. D.; Strain, M. C.; Farkas, O.; Malick, D. K.; Rabuck, A. D.; Raghavachari, K.; Foresman, J. B.; Ortiz, J. V.; Cui, Q.; Baboul, A. G.; Clifford, S.; Cioslowski, J.; Ste-fanov, B. B.; Liu, G.; Liashenko, A.; Piskorz, P.; Komaromi, I.; Martin, R. L.; Fox, D. J.; Keith, T.; Al-Laham, M. A.; Peng, C. Y.; Nanayakkara, A.; Challacombe, M.; Gill, P. M. W.; Johnson, B.; Chen, W.; Wong, M. W.; Gonzalez, C.; Pople, J. A.; Gaussian 09W, Revision D.01, Wallingford, CT, 2009.
[40]. GaussView, Version 5, Dennington, R.; Keith, T.; Millam, J.; Eppinnett, K.; Hovell, W. L.; Gilliland, R. Semichem, Inc., Shawnee Mission, KS, 2009.
[41]. Norret, M.; Makha, M.; Sobolev, A. N.; Raston, C. L. *New J. Chem.* **2008**, *32 (5)*, 808-812.
[42]. Meng, X. X. Applications of Hirshfeld surfaces to ionic and mineral crystals, Ph.D. Thesis, University of New England, 2004.
[43]. Pendas, A. M.; Luana, V.; Pueyo, L.; Francisco, E.; Mori-Sanchez, P. *J. Chem. Phys.* **2002**, *117 (3)*, 1017–1023.
[44]. Desiraju, G. R. *Angew. Chem. Int. Ed.* **2007**, *46 (44)*, 8342–8356.
[45]. CrystalExplorer (Version 3.1), Wolff, S. K., Grimwood, D. J., McKinnon, J. J., Turner, M. J., Jayatilaka, D., Spackman, M. A., University of Western Australia, 2012.
[46]. Sebastian, S.; Sundaraganesan, N. *Spectrochim. Acta A* **2010**, *75 (3)*, 941–952.
[47]. Luque, F. J.; Lopez, J. M.; Orozco, M. *Theor. Chimica. Acta* **2000**, *103 (3–4)*, 343–345.
[48]. Huheey, J. E., Inorganic Chemistry-Principles of Structure and Reactivity, 2nd Edition, Harper Int. Ed., New York, 1978.
[49]. Radovic, L. R.; Bockrath, B. *J. Am. Chem. Soc.* **2005**, *127 (16)*, 5917–5927.
[50]. Thanikaivelan, P.; Subramanian, V.; Raghava Rao, J.; Unni Nair, B. *Chem. Phys. Lett.* **2000**, *323 (1–2)*, 59–70.

Copyright © 2021 by Authors. This work is published and licensed by Atlanta Publishing House LLC, Atlanta, GA, USA. The full terms of this license are available at http://www.eurjchem.com/index.php/eurjchem/pages/view/terms and incorporate the Creative Commons Attribution-Non Commercial (CC BY NC) (International, v4.0) License (http://creativecommons.org/licenses/by-nc/4.0). By accessing the work, you hereby accept the Terms. This is an open access article distributed under the terms and conditions of the CC BY NC License, which permits unrestricted non-commercial use, distribution, and reproduction in any medium, provided the original work is properly cited without any further permission from Atlanta Publishing House LLC (European Journal of Chemistry). No use, distribution or reproduction is permitted which does not comply with these terms. Permissions for commercial use of this work beyond the scope of the License (http://www.eurjchem.com/index.php/eurjchem/pages/view/terms) are administered by Atlanta Publishing House LLC (European Journal of Chemistry).